23rd International Conference on Renewable Energies and Power Quality (ICREPQ'25)
Tenerife (Spain), 25th to 27th June 2025
Renewable Energy and Power Quality Journal (RE&PQJ)
ISSN 2172-038 X, Volume No.23, September 2025

Generalized Predictive Current Control for Grid-Connected Converter with LCL Filter

Martin Bejvl[1], Miroslav Chomát[1], Petr Šimek[1] and Viktor Valouch[1]
[1] Department of Electrotechnics and Electrophysics
Institute of Thermomechanics, Czech Academy of Sciences
Dolejškova 1402/5, 18200, Prague 8 (Czech Republic)
bejvl@it.cas.cz, chomat@it.cas.cz, simek@it.cas.cz, valouch@it.cas.cz

Abstract. The current control based on the GPC (Generalized Predictive Control) algorithm for the power electronic converter connected to the grid via LCL filter is developed. A design process of the control structure and its parameters, and the results of simulation are presented. The current responses to changes in current references and to grid failures are shown and discussed. The algorithm works well also with unbalanced grid voltage. The simplicity and low sensitivity of the basic performance criteria to changes of the LCL filter parameters can be viewed as the important benefit of the strategy developed.

Key words. Generalized predictive current control, grid-connected converter, LCL filter, sensitivity to parameter changes, simulation.

1. Introduction

The Model Predictive Control (MPC) has become popular also in the controllers used in power electronics applications [1]-[5]. A special type of the MPC is the Generalized Predictive Control (GPC). The GPC makes it possible to work with long prediction and/or control horizons [6]. An input-variation term which influences control dynamics is also a part of the GPC. The GPC has been recently used also in the field of the control of power electronic converters.

The current control of the converter with L grid filter using the Generalized Predictive Current Control (GPCC) was developed and tested in [7]-[9]. The power control based on the GPCC applied in the grid-connected converter with L filter was presented in [10].

But, the simplest L filter has low efficiency for suppression of current harmonics. That is the main reason why a more efficient LCL filter is used.

The grid filter structure can be developed according to an acceptable grid current spectrum defined by the IEEE 519-2014 standard in the USA and IEC/TR 61000-3-6:2008 in Europe.

An essential parameter is the rate of the short circuit power at a PCC (Point of Common Coupling) and the nominal power of the converter connected to the PCC. In contribution [11] a possible procedure for the LCL filter design was presented.

Nevertheless, when the full LCL filter topology is considered, it brings some difficulties in the design of current control circuitry. Different control and PWM (Pulse Width Modulation) strategies can be used. Each possible control and PWM strategy has some advantages, but also some disadvantages and limits, [12]-[15]. Among all methods, also the MPC theory has found its application here [16]-[18].

The presented contribution presents an application of the GPCC that has been applied in this area only rarely. Especially, the GPCC applied for the grid-connected voltage source inverter with the LCL filter was presented in [19] for the first time. It was found that the GPCC strategy can be used without the need for any model-based active damping strategy and speed and robustness against model mismatch can be achieved with low computational burden.

Taking into account previous experience in this area, the contribution is focused on using a rather different strategy of generation of the GPCC algorithm than the one presented in [19].

The presented GPCC with short settling times is tested for current control in a voltage converter connected to the grid via LCL filter. A design procedure and results of simulation tests of the GPCC are presented. The presented strategy works well even for unbalanced grid voltages.

The paper is organized as follows: section 2 presents the block diagram of a grid-connected converter and control system; section 3 sets out the equations describing the LCL grid filter between the converter and grid; section 4 summarizes the basic principles of the generalized predictive current control; section 5 presents simulation results for grid-connected converter with the LCL filter, which is controlled by the GPCC strategy; and the conclusions are summarized in the final section 6.

2. Block diagram of grid-connected converter and control system

Figure 1 shows the block diagram of the PWM converter connected to the grid via the LCL filter and with the control of the grid current $\boldsymbol{i}_{L2}$. The reference current components i^*_{L2d}, i^*_{L2q} are transformed to the $\alpha\beta$ static reference frame in which the GPCC is performed as it is shown in section 4. The output converter voltage $\boldsymbol{v}_1$ is generated applying PWM. The controller of the DC voltage v_C is not included in the following analysis and simulation.

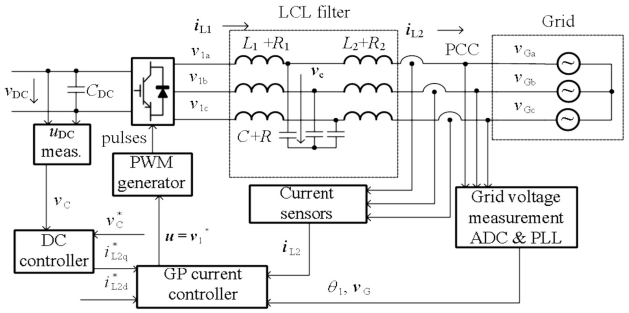

Fig. 1. Block diagram of PWM converter connected to grid via LCL filter and with GPCC of $\boldsymbol{i}_{L2}$.

3. Equations describing LCL grid filter between converter and grid

Contrary to [10] the LCL type of the filter between the converter and the grid is considered here. It is known that for the resonant frequency of the LCL filter ω_{REZ} (its recommended value is 10 $\omega_1 < \omega_{REZ} < \omega_{SW}/2$ where ω_{SW} is switching frequency of the converter) the impedance of the filter is zero and harmonic currents near this frequency are amplified. This effect can be mitigated if some dumping resistances are included into the LCL filter branches. Also the concept of virtual dumping resistances is being used, which results in a control circuitry modification. But, additional sensors must be used in such a case. Thus, the developed GPCC algorithm takes into consideration the resistances in all branches of the LCL filter.

The model of the LCL filter in the Laplace domain is used at the start. After that this model will be transformed into the Z-domain using the Euler backward approximation of the original model in the Laplace domain.

The construction of the model in the Laplace domain is divided into two parts: in the first one the grid voltage $\boldsymbol{v}_g$ is supposed to be zero ($\boldsymbol{v}_g = 0$), in the second one zero output voltage of the converter $\boldsymbol{v}_1$=0.

First part ($\boldsymbol{v}_G$=0):

The parallel combination of capacitor C and inductance L_2 including also respective resistances can be characterized in the Laplace domain as

$$Z_{2C}(s) = \frac{\left[s^2 RCL_2 + s(L_2 + RR_2C) + R_2\right]}{\left[s^2 CL_2 + s(R_2 + R)C + 1\right]} \tag{1}$$

Considering series connection Z_{2C} and inductance L_2 the following equation can be written for the transfer function $\boldsymbol{i}_{L2}(s)/\boldsymbol{v}_1(s)$

$$\frac{\boldsymbol{i}_{L2}(s)}{\boldsymbol{v}_1(s)} = \frac{B_1(s)}{A_1(s)} = \frac{Z_{2C}}{(R_2 + sL_2)\left[(R_1 + sL_1) + Z_{2C}\right]} \tag{2}$$

Second part ($\boldsymbol{v}_1 = 0$):

The parallel combination of capacitor C and inductance L_1 including also respective resistances can be characterized in the Laplace domain as

$$Z_{1C}(s) = \frac{\left[s^2 RCL_1 + s(L_1 + RR_1C) + R_1\right]}{\left[s^2 CL_1 + s(R_1 + R)C + 1\right]} \tag{3}$$

Considering series connection Z_{1C} and inductance L_2 the following equation can be written for the transfer function $\boldsymbol{i}_{L2}(s)/\boldsymbol{v}_G(s)$

$$\frac{\boldsymbol{i}_{L2}(s)}{\boldsymbol{v}_G(s)} = \frac{B_G(s)}{A_G(s)} = -\frac{1}{(R_2 + sL_2) + Z_{1C}} \tag{4}$$

Therefore the following equation can be written for the current $\boldsymbol{i}_{L2}(s)$ after some manipulations and in a shortened form

$$\boldsymbol{i}_{L2}(s) = \boldsymbol{v}_1(s)\frac{b_{21}s^2 + b_{11}s + b_{01}}{a_{41}s^4 + a_{31}s^3 + a_{21}s^2 + a_{11}s + a_{01}} - \boldsymbol{v}_G(s)\frac{b_{2G}s^2 + b_{1G}s + b_{0G}}{a_{3G}s^3 + a_{2G}s^2 + a_{1G}s + a_{0G}} \tag{5}$$

with input variables $\boldsymbol{v}_1(s)$ and $\boldsymbol{v}_G(s)$.

To find the algorithm for the GP current controller in both the axes $\alpha\beta$ of the static reference frame transition to the Z-domain is necessary. For example the Euler backward approximation can be used

$$s \triangleq \frac{1 - z^{-1}}{T_S} \tag{6}$$

Doing that the following equations can be formulated where the coefficients in numerators and denominators are calculated from the respective coefficients of (5)

$$\frac{\boldsymbol{i}_{L2}(z^{-1})}{\boldsymbol{v}_1(z^{-1})} = H_1(z^{-1}) = \frac{B_1(z^{-1})}{A_1(z^{-1})} = \mathbb{Z}\left\{\frac{B_1(s)}{A_1(s)}\right\} = \frac{B_{01} + B_{11}z^{-1} + B_{21}z^{-2}}{A_{01} + A_{11}z^{-1} + A_{21}z^{-2} + A_{31}z^{-3} + A_{41}z^{-4}} \tag{7}$$

and

$$\frac{\boldsymbol{i}_{L2}(z^{-1})}{\boldsymbol{v}_G(z^{-1})} = H_G(z^{-1}) = \frac{B_G(z^{-1})}{A_G(z^{-1})} = \mathbb{Z}\left\{\frac{B_G(s)}{A_G(s)}\right\} = \frac{B_{0G} + B_{1G}z^{-1} + B_{2G}z^{-2}}{A_{0G} + A_{1G}z^{-1} + A_{2G}z^{-2} + A_{3G}z^{-3}} \tag{8}$$

The principle of the GPCC (GP Current Control) of the grid-connected converter will be recapitulated in the following paragraph.

4. Generalized current controller of grid-connected converter.

The GP algorithm will be presented here just in principle because the algorithm was presented in more detail in [7]-[10]. As an example the following equation can be written for the transfer function $i_{L\alpha}/v_{1\alpha}$ in the axis α

$$H_{1\alpha}\left(z^{-1}\right)=\frac{B_1\left(z^{-1}\right)}{A_1\left(z^{-1}\right)}=\frac{i_{L2\alpha}\left(z^{-1}\right)}{v_{1\alpha}\left(z^{-1}\right)}=\frac{y\left(z^{-1}\right)}{u\left(z^{-1}\right)} \tag{9}$$

where the variable $u(z^{-1})$ is the control action and $y(z^{-1})$ is the output of the controlled system.

The controlled object $H_{1\alpha}$ may be characterized by a Controlled Auto Regressive Integral Moving Average (CARIMA) model [7], [8]

$$A_1(z^{-1})y(t)=B_1(z^{-1})u(t-1)+\frac{C(z^{-1})}{\Delta}v(t) \tag{10}$$

where

$$\Delta=1-z^{-1} \tag{11}$$

is the differentiating operator and $v(t)$ is an additive white noise signal. The observer polynomial $C(z^{-1})$ can be written as follows

$$C\left(z^{-1}\right)=1+c_1\left(z^{-1}\right)+c_2\left(z^{-2}\right)+\ldots \tag{12}$$

The objective function J with the control signal u is for the GPC defined

$$J=\sum_{j=1}^{N}\left[\hat{y}(t+j)-y^{*}(t+j)\right]^2+\sum_{j=1}^{N_u}\lambda\left[\Delta u^2(t-1+j)\right] \tag{13}$$

where $\hat{y}(t+j)$ are the j-step ahead predictions of the system output calculated in instant t. They are calculated with regard to the differences of control signal Δu, while $y^{*}(t+j)$ are the future reference outputs of the controlled system. Coefficient N is the prediction horizon, N_u is the control horizon (usually N_u = 1), and λ is the positive weight coefficient. The selection of the parameters N, λ and the polynomial $C(z^{-1})$ influences quality of the control process (stability, bandwidth, settling time, overshoot).

The minimum of the cost function J can be found by making the following gradient equal to zero.

$$\frac{\partial J}{\partial \Delta u}=0 \tag{14}$$

That is the way to find the algorithm for the control signal u generated by the controller. The algorithm for the specific parameters of the LCL filter is given in the following paragraph.

5. Analytical and simulation results.

According to the procedure presented in [11] the design of the LCL filter for the laboratory converter S_A = 20 kVA, V = 400 V, switching frequency f_{SW} = 3 kHz, and for the short circuit power S_{kQ} = 25 MVA was performed.

The parameters of the LCL filter for the nominal grid voltage V_{Gn} may be expressed in % related to the base values (p. u. system)

$$L_b=\frac{Z_b}{\omega_1},\ C_b=\frac{1}{\omega_1 Z_b},\quad \text{where } Z_b=\frac{V_{gn}^2}{S_A} \tag{15}$$

Designing the LCL filter parameters, the following restrictions and recommendations should be followed:

a) $C(\%)<5\%C_b$ (to limit the capacitance reactive power),

b) $L_1+L_2(\%)<10\%L_b$ (to limit the voltage drop),

c) $10\omega_1<\omega_{REZ}<\omega_{SW}/2$,

d) dumping resistor R connected in series with the capacitor C should be so high to make the respective losses acceptable

$$\Delta P_C=\frac{3}{2}R\sum_h\left|\boldsymbol{i}_{L1}(h)-\boldsymbol{i}_{L2}(h)\right|^2 \tag{16}$$

The design of the LCL filter does not represent a straightforward, but iterative process. The LCL filter parameters complying basically the criteria mentioned above are listened in TABLE I where also the parameters of the converter, and voltages used in simulation are listed.

Table I. – Parameters of LCL filter and converter

Inductance L_1 of filter (H)	0.005
Resistance R_1 (Ohm)	1
Inductance L_2 of filter (H)	0.002
Resistance R_2 (Ohm)	0.5
Capacitance C (μF)	20
Resistance R (Ohm)	10
Sampling frequency f_s (Hz)	6000
Switching frequency f_{sw} (Hz)	3000
Grid phase voltage V_{RMS} (V)	115
Converter *dc* bus voltage V_{dc} (V)	400
Delay time $T_d=T_s$ (ms)	1/6

The algorithm parameters N, λ, and the observer polynomial $C(z^{-1})$ should be found in the first step. The simulation of the system shown in Fig. 1 was done in the Matlab™ environment.

Figure 2 presents the relationship among the overshoot Δh_{max} (%) of responses of the current i_α and the coefficients λ and c_2 (N = 5, c_0 = 1, c_1 = 0). The value N = 5 was selected as a good compromise enabling easy selection of the values λ and c_2.

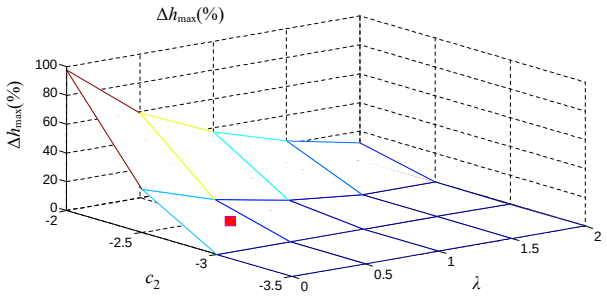

Fig. 2. Overshoot Δh_{max} (%) of current responses for different values of λ and c_2, N = 5. Selected combination of λ and c_2 is marked by small red square.

Figure 3 presents the relationship among the settling time t_S (ms) of the current i_α (the deviation from the set constant value is less than 2 %) and the coefficients λ and c_2 (N=5, c_0=1, c_1=0).

Finally, Fig. 4 presents the relationship among the bandwidth f_{BW} of responses of the current i_α and the coefficients λ and c_2 (N = 5, c_0 = 1, c_1 = 0).

The values c_2 = -2.7 and λ = 0.3 (small red squares in Figs. 2, 3, and 4 indicating the bandwidth f_{BW} = 716 Hz, the settling time t_S = 1.83 ms, and the overshoot Δh_{max} = 3.5 %) were selected for further simulation and investigation as a compromise between the bandwidth and overshoot of the controlled current i_α.

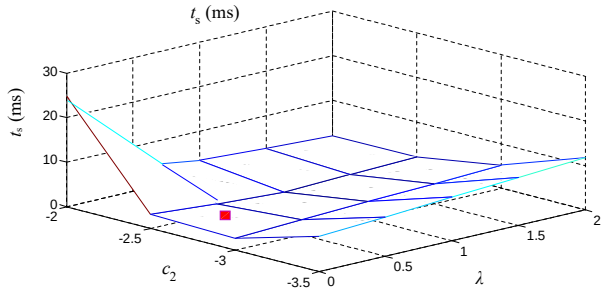

Fig. 3. Settling time t_S (ms) of current responses for different values of λ and c_2, N = 5. Selected combination of λ and c_2 is marked by small red square.

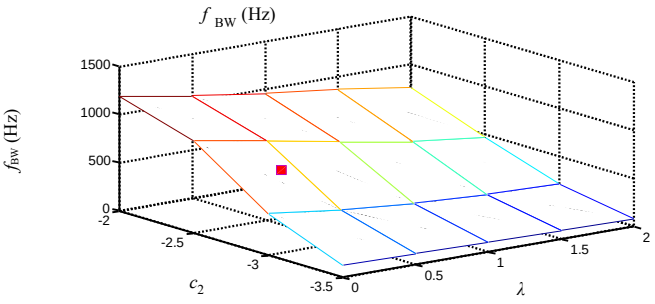

Fig. 4. Bandwidth f_{BW} (Hz) of current responses for different values of λ and c_2, N = 5. Selected combination of λ and c_2 is marked by small red square.

The following expression for the control law $u_\alpha(t)$, considering N=5 and the selected parameters c_2 and λ, was obtained (with the assumption that a simple ZOH circuit with a sampling period T_s is used)

$$\begin{aligned} u_\alpha(t) = {} & 0.8382u_\alpha(t-1)+0.1624u_\alpha(t-2)-9.4881\text{e-}4u_\alpha(t-3)+ \\ & +3.9611\text{e-}4u_\alpha(t-4)-0.4416i_\alpha(t-1)+0.0073i_\alpha(t-2)+ \\ & +0.0377i_\alpha(t-3)+0.2395i_\alpha^{r}(t+2)+0.3015i_\alpha^{r}(t+3)+ \\ & -0.3833i_\alpha^{r}(t+4)+0.2389i_\alpha^{r}(t+5) \end{aligned} \quad (17)$$

and similar one for the control signal $u_\beta(t)$. The values i_α^r are the references for the current at future sampling times.

The sensitivity of the basic performance criteria (Δh_{max}, t_S and f_{BW}) to changes of the parameters of the LCL filter is illustrated in TABLE II. Except of the values of the performance criteria for the basic parameters these values for deviations of ±25 % from the nominal parameter values are presented.

Based on this table, following results can be summarized:

1) all responses are stable for this extent of parameter errors;

2) the sensitivity of all the performance criteria to changes of C, R values is much lower than to changes of the inductances L_1, L_2 with their resistances R_1, R_2;

3) while the performance criteria Δh_{max}, t_S are changing for the better with the increasing values of the LCL parameters, the values of the bandwidth f_{BW} become worse for these parameter changes.

Table II. – Sensitivity of performance criteria to changes of selected LCL filter parameters

changes of parameters		-25%	0	+25%
L_1+R_1	Δh_{max}(%)	14	**3.5**	0
	t_S (ms)	2.33	**1.83**	1.83
	f_{BW} (Hz)	867	**716**	565
L_2+R_2	Δh_{max} (%)	8	**3.5**	0.1
	t_S (ms)	2	**1.83**	1.8
	f_{BW} (Hz)	796	**716**	645
C+R	Δh_{max} (%)	4	**3.5**	3
	t_S (ms)	1.83	**1.83**	1.83
	f_{BW} (Hz)	700	**716**	724

The following figures were obtained by simulation for the system parameters listed in TABLE I and for the constants N = 5, c_2 = -2.7 and λ = 0.3.

Figure 5 shows the responses of the grid and converter voltages and grid currents i_{L2} in both the axes $\alpha\beta$ of the static reference frame after the change from balanced voltage (115-115-115 V_{RMS}) to unbalanced one (V^p_{RMS} = 90 V, V^n_{RMS} =25 V) in t = 0.06 s, and after the change of the reference current $i_{L2}{}^*_{RMS}$ = 20 A to 30 A in t = 0.08 s. The generated converter voltage components represent here the reference signals for the PWM module. That is why also the presented grid current responses are calculated as if the converter generated such ideal voltages. It is obvious that the responses of the grid

current i_{L2} after both the changes are attenuated very quickly in accordance with the data given in TABLE II.

The following Fig. 6 presents the responses of grid currents i_{L2} in the axes $\alpha\beta$ in detail after the changes of all LCL parameters from the nominal ones to only 60% of their values in t = 0.07 s, and after the change of the reference current $i_{L2}{}^{*}{}_{RMS}$ = 20 A to 30 A in t = 0.08 s. The grid voltage v_G is permanently unbalanced in this simulation. The reference values of both the currents in the axes $\alpha\beta$ are presented as well. It is obvious that the actual responses of the grid current components follow their reference signals with delays about 1 ms or even less and without any serious disturbances that are quickly damped after the mentioned changes. It indicates a good resistance of the presented GPCC algorithm to relatively large parameter changes of the control object.

Finally, Fig. 7 shows the converter voltage and grid current responses in the α axis within one fundamental period and also the frequency spectrum of this current.

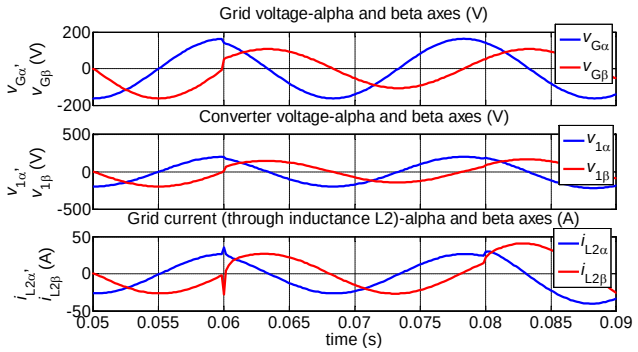

Fig. 5. Responses of grid and converter voltages and grid current i_{L2} in axes $\alpha\beta$ of static reference frame after change from balanced voltage (115-115-115 V_{RMS}) to unbalanced one (V^{p}_{RMS} = 90 V, V^{n}_{RMS} = 25 V) in t = 0.06 s, and after change of reference current $i_{L2}{}^{*}{}_{RMS}$ = 20 A to 30 A in t = 0.08 s.

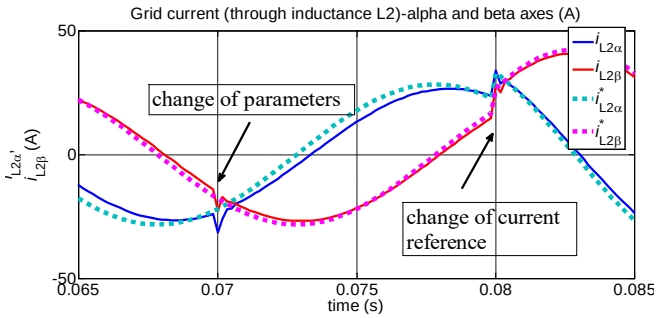

Fig. 6. Responses of grid currents i_{L2} in axes $\alpha\beta$ in detail after changes of all LCL parameters from nominal ones to only 60% of their values in t = 0.07 s, and after change of reference current $i_{L2}{}^{*}{}_{RMS}$ = 20 A to 30 A in t = 0.08 s. Grid voltage v_G is permanently unbalanced

Contrary to the previous two figures the PWM of the converter voltage was assumed. The usual type of modulation, known as the Space Vector Modulation (SVM) was selected. The presented responses are for the balanced grid voltage (115-115-115 V_{RMS}). It is obvious that the highest current harmonic magnitude (the 7th harmonic) is 1.3 % of the magnitude of the fundamental harmonic with frequency 50 Hz. All remaining harmonic components up to 2 kHz are lower than 1 % (except the 11th harmonic they are even lower than 0.5 %).

It is appropriate to recall here that the sampling frequency is only f_S = 6 kHz, so the switching frequency is f_{SW} = 3 kHz owing to the used SVM algorithm. Using other types of the PWM somewhat different harmonic spectra can be obtained.

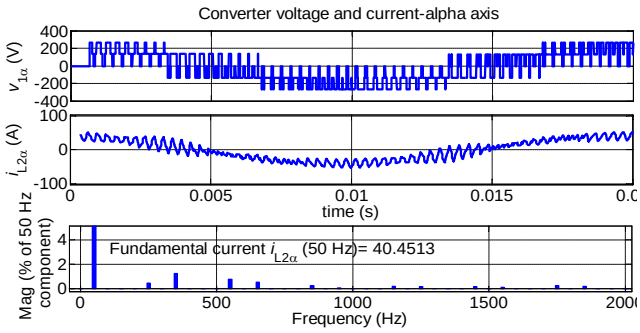

Fig. 7. Converter voltage and grid current responses in α axis within one fundamental period and also frequency spectrum of this current. Responses are for balanced grid voltage (115-115-115 V_{RMS}) and switching frequency f_{SW} = 3 kHz (SVM algorithm used).

6. Conclusion

The GPC based current control for the three-phase voltage source converter connected to the grid via LCL filter was developed, simulated, and tested. The prediction horizon N, weight coefficient λ, and polynomial $C(z^{-1})$, which are the main parameters of the GPC control were designed and examined by simulations. The current responses under different grid failures and for current reference changes were presented and evaluated. The algorithm works well also with unbalanced grid voltage. The simplicity and low sensitivity of the basic performance criteria to changes of the LCL filter parameters can be also viewed as an important benefit of the strategy developed.

Acknowledgement

The authors would like to acknowledge the support from the Institute of Thermomechanics of the Czech Academy of Sciences for its long-term conceptual development, RVO: 61388998.

References

[1] S. Vasquez et al., J.I.Leon, L.G.Franquelo, J. Rodriguez, H.A.Young, A. Marquez "Model predictive control: A review of its applications in power electronics," IEEE Ind. Electron. Mag., vol. 8, no. 1, pp. 16-31, March 2014, DOI: 10.1109/MIE.2013.2290138 .

[2] H. A. Young, M. A. Perez, J. Rodrigues, H. Abu-Rub, "Assesing finite-control-set model predictive control: A comparison with a linear current controller in two-level voltage source inverters," IEEE Ind. Electron. Mag., vol. 8, no. 1, pp. 44-52, March 2014. DOI: 10.1109/MIE.2013.2294870

[3] T. Geyer and D. E. Quevedo, "Performance of multistep finite control set model predictive control for power electronics,"IEEE Trans. Power Electron., vol. 30, no. 3, pp. 1633–1644, Mar. 2015. DOI: 10.1109/TPEL.2014.2316173

[4] Z. Song, Y. Tian, W. Chen, Z. Zou, and Z. Chen, "Predictive duty cycle control of three-phase active-front-end rectifier,"IEEE Trans. Power Electron., vol. 31, no. 1, pp. 698–710, Jan. 2016. DOI: 10.1109/TPEL.2015.2398872

[5] S. Vazquez, J. Rodriguez, M. Rivera, L. G. Franquelo, and M. Norambuena, "Model Predictive Control for Power Converters and

Drives: Advances and Trends," IEEE Trans. Ind. Electron., vol. 64, no. 2, pp. 937, Feb. 2017. DOI: 10.1109/TIE.2016.2625238

[6] Clarke, D. W., Mohtadi, C., Tuffs, P. S., "Generalized predictive control–part I: The basic algorithm," Automatica, vol. 23, no. 2, pp.137-148, 1987. DOI: 10.1016/0005-1098(87)90087-2

[7] Vazques, S., Montero, C., Bordons, C., Franquelo, L., "Design and experimental validation of a model predictive control for a VSI with long prediction horizon," Proc. 39th annual Conf. IEEE Ind. Electr. Society (IECON'13), pp. 5788-5793, Nov. 2013.
DOI: 10.1109/IECON.2013.6700083

[8] Judewicz, M. G., Gonzalez, S. A., Echeveria, N. I. Fischer, J. R., Carrica, D. O.,"Generalized predictive current control (GPCC) for grid-tie three-phase inverters," IEEE Trans. Ind. Electron., vol. 63, no. 7, pp. 4475- 4484, July 2016. DOI: 10.1109/TIE.2015.2508934

[9] M. G. Judewicz, N. I. Echeverria, J. R. Fischer, S. A. Gonzalez and D. O. Carrica," Generalized Predictive Control of Three-Level Boost Rectifiers," XVII Workshop on Information Processing and Control (RPIC), Mar del Plata, Argentina, September 2017. DOI: 10.23919/RPIC.2017.8211626

[10] P. Simek, Bejvl, M., V. Valouch: Power Control for Grid-Connected Converter Based on Generalized Predictive Current Control. IEEE JOURNAL OF EMERGING AND SELECTED TOPICS IN POWER ELECTRONICS, VOL. 10, NO. 6, pp. 7072-7083, DECEMBER 2022, DOI: 10.1109/JESTPE.2022.3208777.

[11] Bejvl, M., Valouch, V.: LCL Filter Design for Interconnection Inverter of Distributed Source to Utility Grids. In Proc. of the 17th Int. Sci. Conf. Electric Power Engineering 2016. Prague, Czech Republic, 16-18 May 2016, ISBN:978-1-5090-0909-1, DOI: 10.1109/EPE.2016.7521832.

[12] Pena-Alzola, R., Lissere, M., Blaabjerg, F., Sebastian, R., Dannehl, J., Fuchs, F. W.: Analysis of the Passive Damping Losses in LCL-Filter-Based Grid Converters. IEEE TRANSACTIONS ON POWER ELECTRONICS, VOL. 28, NO. 6, JUNE 2013, pp. 2642-2646. DOI: 10.1109/TPEL.2012.2222931

[13] Zou, Z., Wang, Z., Cheng, M.: Modeling, Analysis, and Design of Multifunction Grid-Interfaced Inverters With Output LCL Filter. IEEE TRANSACTIONS ON POWER ELECTRONICS, VOL. 29, NO. 7, JULY 2014. pp. 3830-3839. DOI: 10.1109/TPEL.2013.2280724

[14] R. N. Beres, X. Wang, M. Liserre, F. Blaabjerg, and C. L. Bak, "A review of passive power filters for three-phase grid-connected voltage-source converters,"IEEE J. Emerg. Sel. Topics Power Electron., vol. 4, no. 1, pp. 54–69, Mar. 2016. DOI: 10.1109/JESTPE.2015.2507203

[15] Y. Wu, T. B. Soeiro, A. Shekhar, J. Xu and P. Bauer, "Virtual Resistor Active Damping with Selective Harmonics Control of LCL-Filtered VSCs," 2021 IEEE 19th International Power Electronics and Motion Control Conference (PEMC), Gliwice, Poland, 2021, pp. 207-214, DOI: 10.1109/PEMC48073.2021.9432569.

[16] B. Hoff, "Cascaded Model Predictive Control of Grid Connected Converter with LCL Filter," IECON 2018 - 44th Annual Conference of the IEEE Industrial Electronics Society, Washington, DC, USA, 2018, pp. 5277-5282, DOI: 10.1109/IECON.2018.8591137.

[17] T. Dragičević, C. Zheng, J. Rodriguez, and F. Blaabjerg, "Robust QuasiPredictive Control of LCL-Filtered Grid Converters," in IEEE Transactions on Power Electronics, vol. 35, no. 2, pp. 1934-1946, Feb. 2020, DOI: 10.1109/TPEL.2019.2916604.

[18] T. Zhao, M. Zhang, C. Wang, and Q. Sun, "Model-Free Predictive Current Control of Three-Level Grid-Connected Inverters With LCL Filters Based on Kalman Filter," in IEEE Access, vol. 11, pp. 21631-21640, 2023, DOI: 10.1109/ACCESS.2023.3251410.

[19] M. G. Judewicz, S. A. González , J. R. Fischer , Juan F. Martínez, and D. O. Carrica," Inverter-Side Current Control of Grid-Connected Voltage Source Inverters With LCL Filter Based on Generalized Predictive Control," IEEE Journal of Emerging and Selected Topics in Power Electronics, Volume. 6, no. 4, December 2018, DOI: 10.1109/JESTPE.2018.2826365